

Cellulose Nanopaper with Monolithically Integrated Conductive Micropatterns

Alireza Hajian, Zhen Wang, Lars A. Berglund, and Mahiar M. Hamedī*


This work presents a route to fabricate micropatterned conductive structures where the conductors are monolithically integrated with nanocellulose-based paper. To fabricate conductive features, microstructures are patterned on filter papers using wax-printing, followed by vacuum filtration of carbon nanotubes (CNTs) or silver nanowires (AgNWs) dispersed in aqueous cellulose nanofibrils (CNFs). These patterns are then laminated onto a pure CNF substrate (both in gel-state) and dried to form cellulose nanopapers with integrated conductive micropatterns. Resolutions of the conductive features are shown down to 400 μm wide, 250 nm thick, and with conductivity values of $115 \pm 5 \text{ S cm}^{-1}$ for the CNF–CNT and $3770 \pm 230 \text{ S cm}^{-1}$ for the CNF–AgNW micropatterns. The nanopaper and the conductive patterns both constitute random fibrous networks, and they display similar ductility and swelling behavior in water. Thus, the integrated conductive micropatterns can withstand folding, as well as wetting cycles. This stability of the micropatterns makes them useful in various devices based on nanocellulose substrates. As an example, an electroanalytical nanopaper device that operates in wet conditions is demonstrated.

1. Introduction

In printed electronics, conductive patterns are printed on an insulating substrate, e.g., polymers or paper.^[1] The main fabrication methods for printed electronics are based on direct printing, spray deposition, sputtering, or stamping on a premade substrate (synthetic polymers, glass, or paper).^[2–7] These methods are mainly suitable for making thin films with thicknesses of around 100 nm, and thicker conductive patterns are harder to fabricate.^[8–11] Furthermore, the conductive patterns and the substrates usually constitute two different classes of materials (e.g., metal or carbon particles deposited on polymers or papers), and the incompatibility between the substrate and the pattern in terms of mechanical or physical properties (e.g., swelling ratio in contact with a solvent) is a challenge.

Dr. A. Hajian, Dr. Z. Wang, Prof. L. A. Berglund, Dr. M. M. Hamedī
 Department of Fiber and Polymer Technology
 KTH Royal Institute of Technology
 Teknikringen 56, 100-44 Stockholm, Sweden
 E-mail: mahiar@kth.se

Dr. A. Hajian, Prof. L. A. Berglund
 Wallenberg Wood Science Centre
 KTH Royal Institute of Technology
 Teknikringen 56, 100-44 Stockholm, Sweden

 The ORCID identification number(s) for the author(s) of this article can be found under <https://doi.org/10.1002/aelm.201800924>.

DOI: 10.1002/aelm.201800924

More specifically in paper-based electronics, usually, thin films of conductive materials are patterned by direct printing on paper.^[12] Paper as a substrate contains a random network of cellulose fibers. Due to the macroporous network of fibers in the paper, it is challenging to print thin films of polymers and metals on unmodified paper. Furthermore, paper is not optically transparent compared to most polymeric sheets,^[8,13] which limits its application in electronic devices that require transparency.

An alternative to cellulose paper is a cellulose nanopaper. A nanopaper consists of a nanostructured random network of cellulose nanofibrils (CNFs). Nanopaper has four interesting properties: i) It has a nanoscale porosity, ii) It has a high optical transparency, in both the visible and ultraviolet spectra. iii) It has a low (nanoscale) surface roughness. iv) It has a higher Young's modulus and a higher

strength value than most plastic substrates.^[14–18] Cellulose nanopaper has, therefore, also been considered as a substrate in printed electronics^[19–24] where mostly metallic nanoparticles (Ag or Au) have been printed on a prefabricated nanopaper, for example using sputtering to form thin films (below 100 nm) with lateral resolutions in the micrometer dimensions.^[25,20] Metallic patterns have the advantage of providing a high conductivity, however, sputtering can be a time-consuming and expensive process, and poor adhesion between the metallic particles with paper or plastics can be an issue that deteriorates the performance of the conductive pattern during handling and deformation.^[26] Metallic nanoparticles, furthermore, need to be sintered through heating to obtain a high conductivity.^[27,28] A major obstacle for printing on cellulose nanopaper, however, is the hygroexpansion of nanopaper (CNF nanopaper swells up to 50 times in water^[29]). For this reason, previous work has relied on nonwater based inks for inkjet printing on nanopaper.^[25] Additionally, the difference between the swelling behavior of nanopaper and the coated layer can lead to cracks or detachment of the coating. Folding of patterned nanopaper can also lead to cracks or detachment of the coated layer.^[30]

In this work, we have developed a process that monolithically integrates printed micropatterned electronic structures and cellulose nanopaper. This process relies on the ability of CNFs to disperse functional nanomaterials in water, such as metal nanowires,^[31,32] nanosheets^[33] and unmodified CNTs,^[34,35] or conducting polymers.^[36,37] The codispersions of CNF and functional nanomaterials enable fabrication of composites

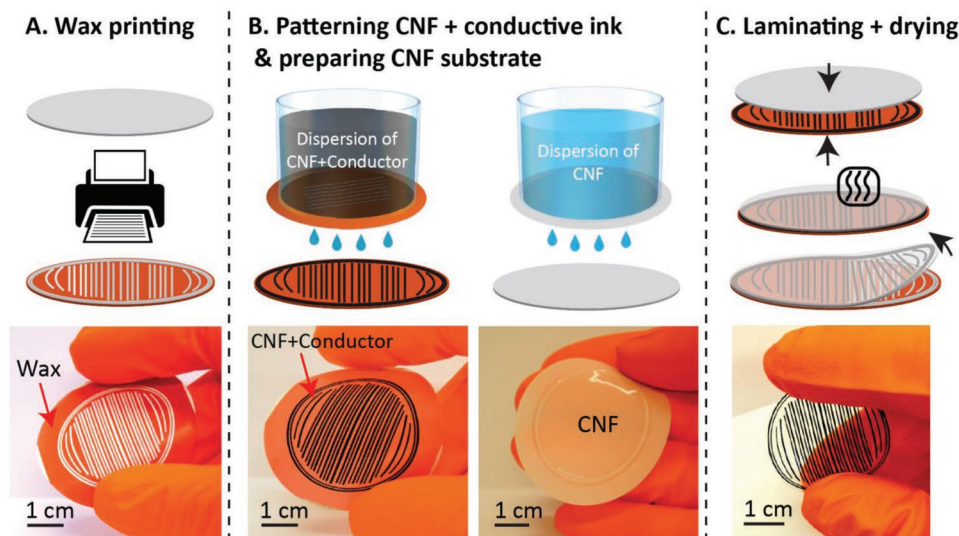


Figure 1. Schematic diagrams and photographs show the procedure for fabricating micropatterned conductive nanopaper composites: A) Wax (orange color) is printed onto a filter paper. B) Vacuum filtration of dispersions of CNFs that contain either CNTs or AgNWs through the wax printed filter paper. In parallel, pure CNF dispersions are filtered through a neat filter paper to form the nanopaper substrate. These filtered dispersions form hydrogels on the filter paper as seen from the two photographs in the middle. C) The hydrogels on the filter paper are laminated, vacuum pressed and dried. The nanopaper is finally removed from the filter paper to form a freestanding patterned structure (photograph on the bottom right).

with various functionalities. Conductive nanopapers can be fabricated directly from codispersions of CNF and functional nanomaterials, using the identical process to that used for making the CNF nanopapers (i.e., vacuum filtration followed by drying),^[38] and result in a film with a random fibrous network.^[39] We show that this fabrication process allows the micropatterning of complex conductive shapes with different thicknesses (250 nm to 5 μm), and results in structures with similar ductility and swelling behavior as that of pure cellulose nanopaper.

2. Results and Discussion

We prepared negatively charged (1200 $\mu\text{equiv g}^{-1}$) CNFs^[40] (see the Experimental Section) and used the ability of CNFs to disperse other nanoparticles (as previously described by us and others) to prepare dispersions of as-prepared multiwalled carbon nanotubes (CNTs) with 60 wt% CNTs, or silver nanowires (AgNWs) with 60 wt% Ag, in water (see the Experimental Section).^[31,34,35] We chose multiwalled CNTs because their production price is an order of magnitude lower than single-walled CNTs,^[41] and they can be used as inert electrodes in various applications (AgNWs can be oxidized under air and ultraviolet exposure^[31]). We chose AgNWs because they have much higher conductivity than CNTs which makes them suitable for electrical wires (e.g., in printed circuit boards).^[42–44]

Particles dispersed in water can be micro-patterned by passing them through a wax-printed filter. In a previous report, a wax-patterned paper was used to co-fabricate microfluidics and electronics on paper by forming a hydrophobic coating inside paper microchannels.^[45] Wax printing and vacuum filtration of an aqueous AgNW dispersion have also been used to form a conductive pattern onto a polymer substrate.^[46]

Drop-casting or vacuum filtration of aqueous AgNWs or CNTs has been used to fabricate uniform conductive coating on cellulose nanopaper.^[21,47] Here, we used a wax printer to form micropatterns on filter papers. **Figure 1** shows the patterning process: when the aqueous dispersion of nanoparticles is vacuum-filtered through the wax-printed filters, the dispersion passes through the unwaxed parts (due to the hydrophobicity of wax) and forms a stable gel. This composite hydrogel contains around 20 wt% solid content. In parallel, we prepared a pure CNF gel by vacuum filtration of the CNF dispersion using a neat filter paper (Figure 1B). After filtration, we laminated and press-dried the pure CNF hydrogel and the patterned hydrogel of CNF–CNTs or CNF–AgNWs. We removed the waxed filter paper leaving a semidried micropattern of CNF–CNTs/AgNWs that was adsorbed to the CNF gel, and the wet patterned structure was completely dried using a sheet forming machine (see Figure 1C and the Experimental Section). This technique caused the conductive patterns to penetrate into the bulk of the nanopaper and form monolithically integrated micropatterns (see Figure S14 in the Supporting Information).

The resolution of the conductive features depends on the resolution of the printer, which was 400 μm in this study. **Figure 2A** shows the transparency of the CNF substrate in which the dark micropatterned CNF–CNTs are visible (against a colorful background). In Figure 2B,G, top-view scanning electron microscopy (SEM) image from the edge of the patterned features shows a distinct edge (between CNFs and CNF–CNTs, or CNF–AgNWs). The patterned parts that contain 60 wt% CNTs, or AgNWs display mostly larger CNT, or AgNW particles network, while the CNF side contains only nanocellulose particles that form a densely packed network (SEM images in Figure 2B,G). We could control the thickness by decreasing the amount of the dispersion (or by diluting the dispersions in water) to be filtered, and demonstrated the lowest thickness of

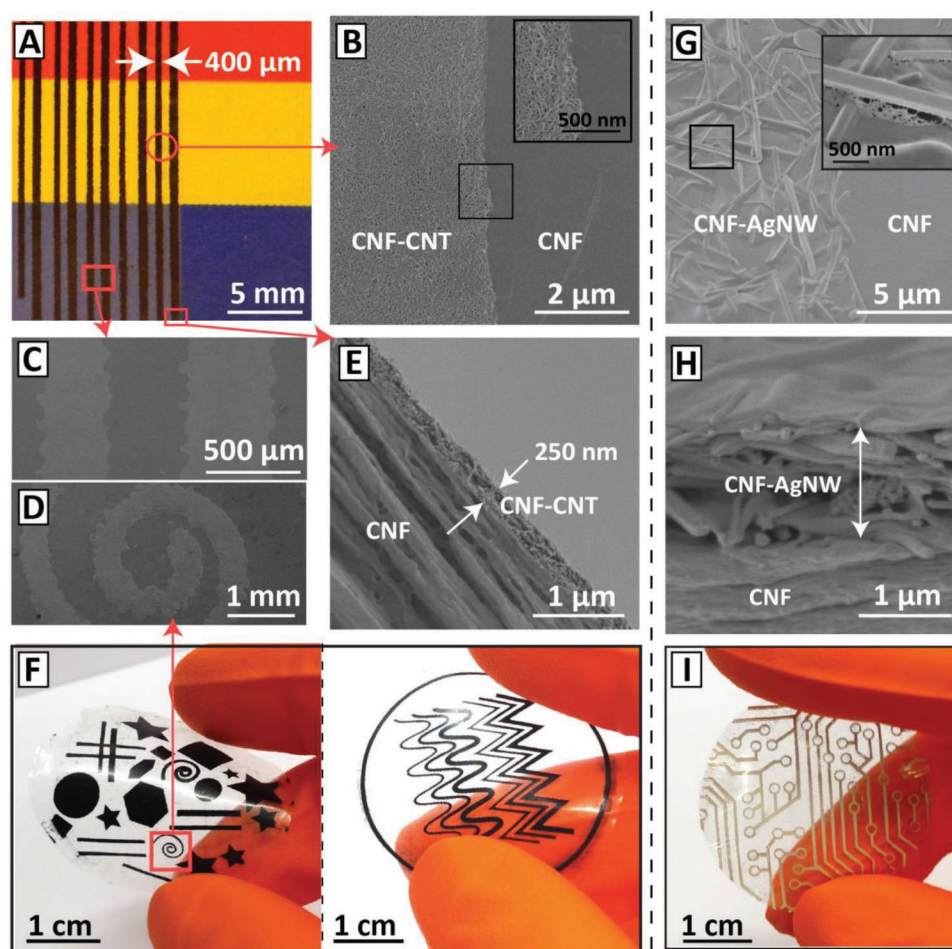


Figure 2. A) An optical image of a micropatterned nanopaper against a colorful background shows the transparency of the nanopaper and the resolution of CNF–CNT structures down to 400 μm . B) Top-view SEM image from the edge of the patterned CNT line shows distinguishable CNF and CNF–CNT parts (the inset shows a higher magnification). C,D) SEM images from the parallel lines and the spiral feature. E) Cross-sectional SEM image of a CNF–CNT pattern embedded into the CNF substrate with a thickness of 250 nm. F) Photographs of nanopapers with various integrated CNF–CNT micropatterns. G) Top-view SEM image from the edge of a CNF–AgNW line (inset shows a higher magnification). H) Cross-sectional SEM image of a CNF–AgNW pattern embedded into the CNF substrate with a thickness of 1 μm . I) A photograph of a nanopaper with micropatterned CNF–AgNWs.

250 \pm 25 nm for CNF–CNTs and 1 μm for CNF–AgNWs, and the highest thickness of more than 1 and 5 μm , respectively (see Figure 2E,H, and Figures S2 and S12 in the Supporting Information). This fabrication method can achieve a greater range of thickness in a single processing route compared to printing conductive patterns (e.g., AgNWs on polydimethylsiloxane,^[46] graphene on glassine paper,^[8] or sputtering on cellulose nanopaper).^[25] The micropatterned features are not limited to straight lines and various complex shapes with bent and sharp edges can be made (Figure 2F,I and Figure S1, Supporting Information). The patterned features were embedded in the bulk of the substrate which resulted in an overall flat surface as measured by atomic force microscopy (AFM) (see Figure S6 in the Supporting Information).

We measured the conductivity of the CNF–CNT patterns to $115 \pm 5 \text{ S cm}^{-1}$ and CNF–AgNW patterns to $3772 \pm 232 \text{ S cm}^{-1}$. The conductivity of CNF–AgNW patterns is comparable to previously reported AgNWs coated on CNF nanopaper, considering that the composite patterns in this work contain only 60 wt%

AgNWs.^[31,48] The conductivity of the CNF–CNT patterns is in a higher range than most previously reported carbon-based printed electronics.^[8,21,49,50] This high conductivity can be attributed to the efficiency of CNFs to disperse unmodified CNTs in water.^[35] This method preserves the pristine structure of the CNTs, avoids chemical functionalization which can damage the electronic structure of the CNTs, and also avoids the use of surfactants which can perturb the CNT–CNT contacts.

The change of the CNF–CNT or CNF–AgNW thickness did not alter the conductivity of the patterns which suggests that the homogeneity of the pattern is independent of the initial concentration of the dispersion (different particle concentration but the same CNT or AgNW wt%) and also independent of the pattern thickness (Figure 3A). The resistivity of the micropatterned structures increased linearly with an increasing length of the patterns, (Figure 3B). This linear relation is also indicative of a homogeneous CNTs/AgNWs network in the conductive features.

To test the folding tolerance of the conductive patterns, we performed folding–unfolding test and measured conductivity

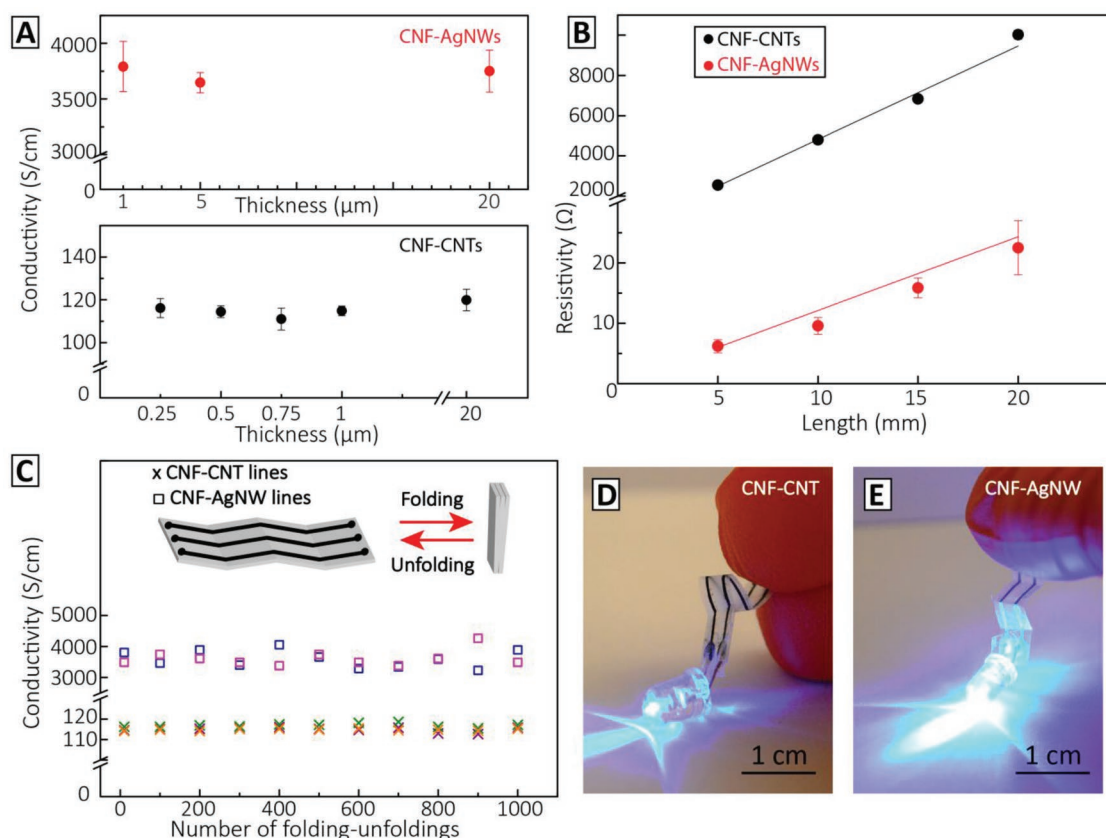


Figure 3. A) Conductivity versus thickness for micropatterned CNF-AgNWs (top) and CNF-CNT lines (bottom) with different thicknesses. B) Resistivity of the micropatterned CNF-CNT features with 250 nm thickness and CNF-AgNWs with 5 μm thickness both showing a linear increase with increasing length of the line. C) The conductivity of the CNF-CNT (cross symbols) or CNF-AgNW (square symbols) micropatterned lines versus folding-unfolding cycles, where three folded lines were tested along each line and folded from -180° to 180° . Each color represents data for an individual line. D,E) Photographs of folded micropatterned lines (contain CNTs or AgNWs) that are connected to a 9 V battery and deliver power to LEDs.

after each 100 folding-unfolding cycles (see the Experimental Section). The results based on 3-point folding in Figure 3C (that includes folding in both 180° and -180°) show that there is no change in the conductivity of the patterns after 1000 folding-unfolding cycles (previous reports on folding tolerance with metallic or carbon-based nanoparticles as the conductive coating showed a reduction in conductivity).^[8,51,52] We connected two CNF-CNT conductive lines, with 250 nm in thickness and 600 μm in width, a resistance of $10 \pm 0.4 \text{ k}\Omega$, to a light emitting diode (LED). The LED could emit light (when connected to a battery), even during folding-unfolding cycles (Figure 3D). We could lower down the resistance of the lines in Figure 3E to $22 \pm 5 \text{ }\Omega$ with fabricating 5 μm thick CNF-AgNW patterns (Figure 3B and Figure S12, Supporting Information). The AgNW patterns were also resilient toward folding similar to the CNF-CNT patterns.

To better understand the folding resilience of the micropatterned structures, we analyzed the mechanical and electrical properties of the nanopapers as bulk composites to find similarities in the mechanical performance of the substrate (CNF nanopaper) and the conductive pattern (CNF-multiwalled CNT composite nanopapers). We fabricated nanopapers with different ratios between CNFs and CNTs, and with an average thickness of 20 μm (see the Experimental Section

and Figure 4A). The electrical conductivity of the composite nanopapers follows a power law model with low regression in logarithmic scale which suggests that the formation of aggregates can be neglected (Figure 4B). Moreover, dynamic light scattering data comparing CNF and CNF-60 wt% CNTs dispersions in water, qualitatively display the same homogeneity in the distribution of the particles (Figure S7, Supporting Information).

An increase in the CNT content above 20 wt% caused an increase in the porosity of the composite nanopaper, while the apparent density was almost unaltered in all compositions (1.5 g cm^{-3} on average; Table S1, Supporting Information). In a random fibrous network of straight rods, the total number of fiber crossings (N_c) in a 2D area (A) can be computed as^[53]

$$N_c = \frac{L_f^2 N_f^2}{\pi A} \quad (1)$$

where L_f is the average fiber length and N_f is the number of fibers. If we assume the same length for CNTs and CNFs (2 μm), then fewer CNT particles (with an average diameter of 7.5 nm) are present in a unit area of the network than the thinner CNFs (3 nm in diameter). Therefore, the number of fiber crossings in the CNF-CNT nanopaper with high CNT content becomes

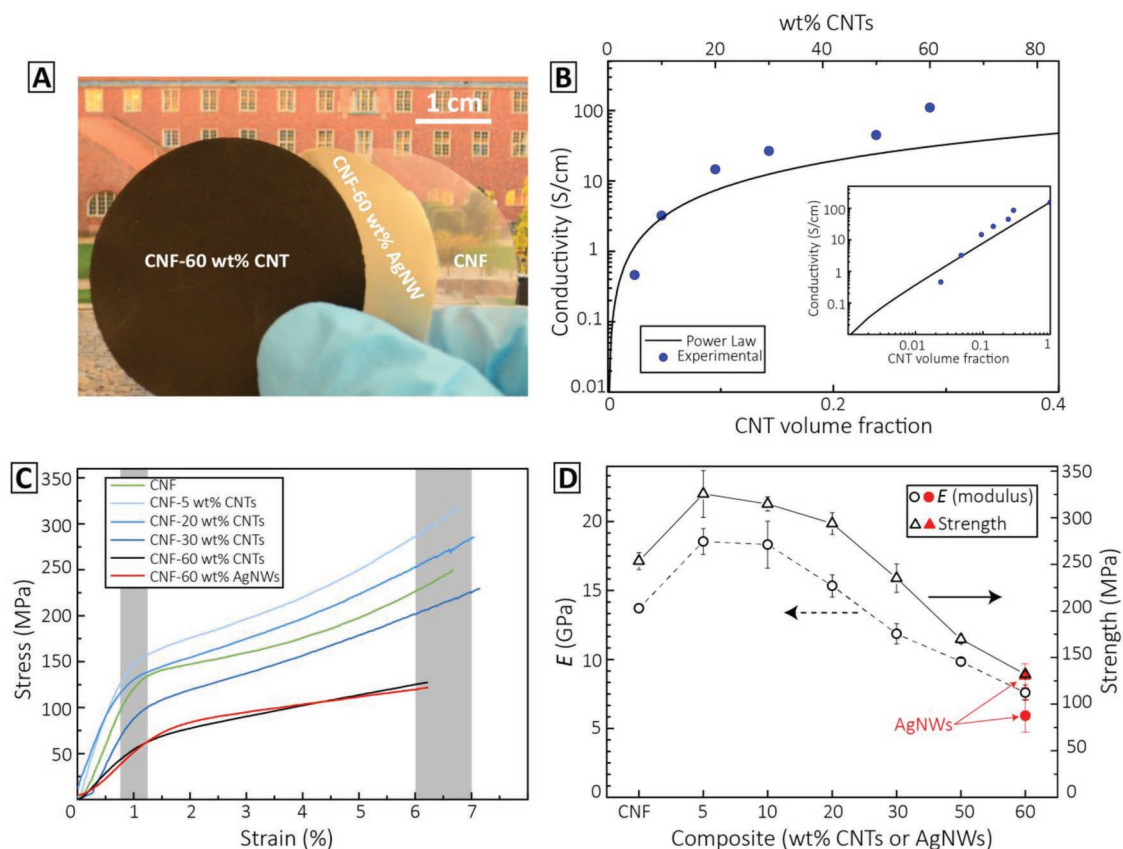


Figure 4. A) A photograph of the nanopapers (CNF on the right, CNF-60 wt% AgNWs in the middle and CNF-60 wt% CNTs on the left). B) The electrical conductivity of the composite nanopapers with different CNT volume fraction fitted with a power law model. The inset shows logarithmic scale fitting which shows a linear relation. C) Typical tensile stress–strain graphs of the composite nanopapers with different CNT wt% and with 60 wt% AgNWs. The gray regions around 1% and 6–7% show the typical yield strain and strain at break, respectively. D) Young's modulus and strength of the composite nanopapers versus CNT wt% (empty black symbols) or 60 wt% AgNWs (filled red symbols).

less than the pure CNF nanopaper. The fiber–fiber bonding is also stronger among the CNFs compared to the unmodified CNTs.^[53,54] In a nonentangled random fiber network, weak points commonly arise from the junctions (fiber crossings), where load transfer among the fibrils occurs. Therefore, we can assume CNT–CNT contacts as soft domains and CNF–CNF contacts as hard domains. In the composites with 5 or 10 wt% CNTs, most of the fiber junctions are CNF–CNF contacts combined with strong fiber bonding between the CNTs and the CNFs (because of the presence of charged groups on CNF surface as discussed elsewhere^[35]). This can explain increased Young's modulus and strength for low CNT content nanopapers (below 20 wt% CNTs), considering the negligible porosity of 3–4% and similar density of around 1.5 g cm^{-3} . The electrical conductivity values of the composite nanopapers with different CNT volume fractions (Figure 4B) show that—above 30 wt% CNTs—a spanning cluster of the CNTs network form (start of plateau region in the graph) where most of the fiber crossings in the composite network are governed by CNT–CNT contacts. The plateau region shows reaching the maximum conductivity that can be obtained in a composite. Thus, above 30 wt% CNTs, the strain energy is predominantly stored in the soft regions (according to mechanics of random fiber networks).^[55] One explanation for the reduction in modulus and strength in

Figure 4D can be the reduced number of fiber crossings and the forces that govern at these crossings.^[53,54] The yield strain and strain at break, however, are similar for different compositions, and their stress–strain graphs show similar elastic behavior to a CNF random fibrous network (Figure 4C). For example, a comparison between CNF and the composite nanopaper containing 60 wt% CNTs or AgNWs, shows yield strain values of around 1% and strain at break values below 6.5% (see gray areas in Figure 4C). The lower Young's modulus (E) for the 60 wt% AgNWs composite (filled red circle in Figure 4D) can be explained by higher porosity of the AgNW composites (Table S1, Supporting Information). We used AgNWs with an average length of $35 \mu\text{m}$, and an average diameter of 135 nm (see the Experimental Section). Larger AgNWs will, therefore, have less number of fibers in a unit area and less number of fiber contacts compared to the CNTs. The higher mass density of the AgNWs, however, seems to compensate for this fewer number of contact points, and the composite nanopapers with 60 wt% AgNWs, therefore, show similar strength (filled red triangle in Figure 4D) with only 1.5 GPa lower Young's modulus compared to those with 60 wt% CNTs.

All these factors combined with the similar tensile property data and relative homogenous particles distribution in the dispersions (see Figures S7 and S9 in the Supporting Information)

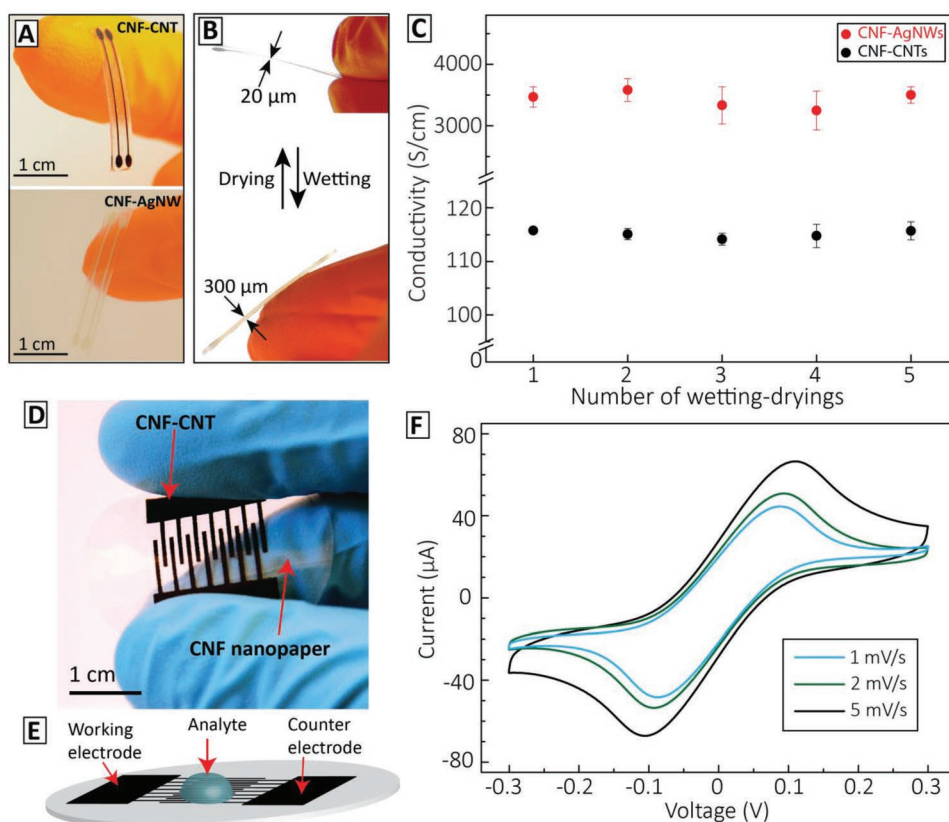


Figure 5. A) Photographs of micropatterned lines of CNF–CNTs and CNF–AgNWs after immersion in water. B) Photographs show the thickness of the nanopaper in both dry state and in fully swollen (wet) state. C) The conductivity of the patterns after each wetting–drying cycle shows stable conductivity after 5 cycles. D) A photograph of interdigitated symmetrical CNF–CNT electrodes, where CNF is the insulating substrate and as the separator for CNF–CNTs as conductors. E) Schematic diagram of the structure in (D) used as an electroanalytical device. F) Cyclic voltammograms measured using the patterned structure in (D) at three different scan rates of 100×10^{-3} M potassium ferrocyanide in $1 \times$ PBS as the analyte.

suggest that CNF–CNT or CNF–AgNW nanopapers have similar elastic behavior and ductility to pure CNF nanopaper. This similarity in mechanical properties prevents damage to the conductive patterns during folding.

Probably the most important feature of the micropatterned nanopapers is its resilience against hygroexpansion. To test the stability of the micropatterns against hygroexpansion, we performed cyclic wet-stability tests (by immersing the structure in water for 10 h then drying using the sheet former). **Figure 5A** shows the stability of the patterns after cyclic immersion in water. Due to the hydrophilic surface and similar swelling of the CNF and CNF–CNT/AgNW composites, both structures swell in water without any damage to the patterns. This swelling, however, is negligible in the in-plane direction and primarily occurs out-of-plane of the nanopaper, because of the 2D fibrous structure of the nanopapers (Figure 5A,B and Figure S10, Supporting Information). Wetting of the micropatterned nanopaper resulted in 15-fold increase in weight and thickness. Drying the wet-patterned nanopapers resulted in the same initial structure, with retained dimensions and conductivities (Figure 5C). This stability cannot be achieved by using, for example, metallic particles coated on CNF nanopaper due to the different swelling ratios between the substrate and the coating.^[25,29] Nevertheless, in this work, due to the attachment of the CNF network to the surface of AgNWs (inset in

Figure 2G and Figure S13 of the Supporting Information), and the embedding of the AgNWs in the bulk of CNF network, the structures were resilient to swelling in water and to drying (Figure 5A,B). The dry AgNW micropatterns had a conductivity of $3500 \pm 130 \text{ S cm}^{-1}$, even after 5 wetting–drying cycles (red symbols in Figure 5C).

To test the electrical performance of the conductive micropatterns in wet conditions, we fabricated an electroanalytical device. This device as shown in Figure 5D contains patterns of symmetrical interdigitated CNF–CNT electrodes. The interdigitated arrays have a width of $500 \mu\text{m}$ and a length of 1 cm, and a separation distance between the lines of $500 \mu\text{m}$. Using these electrodes, we analyzed the reversible redox system of $[\text{Fe}^{\text{III}}(\text{CN})_6]^{3-}/[\text{Fe}^{\text{II}}(\text{CN})_6]^{4-}$ (potassium ferri/ferrocyanide in $1 \times$ phosphate-buffered saline, PBS) coupled with cyclic voltammetry (CV) at different scan rates. We dropped 1–2 droplets of the analyte solution on the interdigitated lines that were connected to the electrodes (see Figure 5E and the Experimental Section). CV graphs at different scan rates of 1, 2, and 5 mV s^{-1} in Figure 5F show pairs of redox peaks as a result of the redox reactions occur between $[\text{Fe}^{\text{III}}(\text{CN})_6]^{3-}/[\text{Fe}^{\text{II}}(\text{CN})_6]^{4-}$. At the scan rate of 5 mV s^{-1} , we calculated the formal reduction potential ($E^0 = (E_a + E_c)/2$, where E_a is the anodic peak potential and E_c is the cathodic peak potential) as 2.64 mV versus CNF–CNT quasi-reference.

The separation of the peak potentials ($\Delta E_p = E_a - E_c$) is 214 mV which corresponds to the number of electrons involved ($n = 59 \text{ mV}/\Delta E_p$) in this redox reaction of 0.28. ΔE_p increases along with scan rate: 176 mV at 1 mV s^{-1} , 185 mV at 2 mV s^{-1} , and 214 mV at 5 mV s^{-1} .^[56] The ratios of cathodic and anodic peak currents (1.08 at 1 mV s^{-1} , 1.05 at 2 mV s^{-1} , and 1.01 at 5 mV s^{-1}) are close to unity. These ratios indicate that the redox processes are almost reversible with no other redox reactions except the $[\text{Fe}^{\text{III}}(\text{CN})_6]^{3-}/[\text{Fe}^{\text{II}}(\text{CN})_6]^{4-}$ couple between the electrodes. It should be noted that the reversibility of the redox reaction, as a performance indicator of the sensor built with CNF–CNT composite, varies when evaluated according to the potentials or the currents.^[37] We attribute this difference to the fact that the potential values in here are recorded with a quasi-reference (CNF–CNT). Most importantly, these results show that micropatterned electrodes can operate in wet state even considering the large swelling ratio showed earlier, which opens up possibilities for using cellulose nanopaper devices for aqueous electrochemical sensing.

3. Conclusions

We have demonstrated a fabrication method for co-fabricating micropatterned conductive features of CNF–CNT, or CNF–AgNW and nanopaper using combined wax printing and filtration technique. These micropatterned conductors are monolithically integrated into the cellulose nanopaper, and have six advantages: i) The thickness of the conductive features can be adjusted by varying the CNF–CNTs/AgNWs concentration (we could fabricate patterns with thicknesses between 250 nm, up to 5 μm). ii) The CNF–CNT/AgNW micropatterns are embedded in the bulk of the nanopaper, resulting in a flat surface. iii) Many shapes can be fabricated simply by using wax printing. The resolution of the micropatterns is defined by the printer (the lowest resolution was 400 μm in this study). iv) The integrated conductors do not alter the strength of the nanopaper, which showed an average strength of 253 MPa and a modulus of 13.7 GPa). v) The conductive features can reach high conductivity values, because the CNF is an efficient dispersing agent for such nanoparticles (115 S cm^{-1} for CNTs and 3700 S cm^{-1} for AgNWs). vi) The monolithic integration and the mechanical compatibility between the micropatterned CNF–CNT/AgNW and the pure CNF substrates lead to conductive micropatterns that are highly resilient to folding, and more importantly resilient to hygroexpansion (nanopaper expands 15 times when wetted). To demonstrate the usability of resilience to hygroexpansion, we fabricated an electroanalytical device with micropatterned CNF–CNT interdigitated electrodes.

This work shows a step towards a fast and simple route to fabricate conductive micropatterns integrated with nanocellulose substrates. These patterns can be used for different printed electronic devices and they can also operate in wet conditions. This technique should not be limited to CNTs or AgNWs, and should be applicable to other functional nanoparticles and materials that can be dispersed or mixed with CNFs.^[33,37,50] Nanopaper-based microelectronics could find uses in analytical devices in vivo or in vitro,^[57,58] cellulose

microfluidics,^[59–61] cellulose-based optical devices,^[62,63] and printed microbatteries.^[64]

4. Experimental Section

Preparation of Dispersions: Negatively charged CNFs were prepared using TEMPO (2,2,6,6-tetramethylpiperidine-1-oxyl radical)-mediated (Sigma Aldrich) oxidation of softwood sulfite dissolving pulp, as described in a previous report.^[40] CNF–CNT dispersions were prepared by adding as-prepared multiwalled CNTs powder (Sigma-Aldrich, Production code: 724769) to a 1 g L^{-1} CNF aqueous dispersion followed by sonication at 750 W and 50% amplitude in ice bath with a probe tip diameter of 12 mm for 20 min using Vibra-Cell CV33 (Sonics & Materials Inc., Newton, USA), and centrifugation at $20\,000 \times g$ using Beckman Coulter J2 for 90 min. After centrifugation, 80% of the resultant supernatant was taken out and CNT wt% was calculated based on Beer–Lambert law and according to previous reports.^[34,35]

Fabrication of Nanopapers: The 1 g L^{-1} CNF and hybrid dispersions were vacuum filtered using hydrophobic polyvinylidene difluoride (PVDF) Millipore membrane filters with a 0.65 μm pore size (Durapore, Merck Millipore, Darmstadt, Germany) followed by sheet forming using Rapid Köthen, RK3A-KWT PTI at a vacuum pressure of -1 bar at 90°C for 15 min.

Patterning on CNF Nanopapers: The patterns using a wax printer were designed, where a layer of wax was printed on a PVDF filter paper with a Xerox ColorQube wax printer, and these wax-patterned filter papers were used to vacuum filter the conductive ink (aqueous CNF–CNTs dispersion) until a wet-gel is formed on top. Due to wax hydrophobicity, the aqueous dispersion did not adhere to the wax and passed through the unwaxed parts and the wet gel was formed on those areas. At the same time, the earlier-prepared CNF dispersion was vacuum filtered on a bare PVDF filter paper until a wet-gel was formed. Depending on the desired pattern thickness, CNF–CNT dispersions were vacuum filtered with a concentration between 0.05 and 0.5 g L^{-1} and with a volume of 5–15 mL. The filtration diameter was 40 mm and the basis dry weight of the nanopaper was around 30 mg. Next, the two gels were placed on top of each other followed by sheet forming using Rapid Köthen, RK3A-KWT PTI at a vacuum pressure of -1 bar at 90°C in 2 steps: i) for 3 min until the CNF–CNT gel was adsorbed/penetrated into the CNF nanopaper but not completely dried. Next, the waxed filter paper was removed. This short-step drying prevents melting of the wax and contamination. ii) 10 min drying until it was completely dried.

Tensile Testing: Tensile testing of nanopapers was performed using Universal Material Testing Machine Instron 5944 (Norwood, MA, USA) equipped with 500 N load cell with a strain rate of $10\% \text{ min}^{-1}$. 5 specimens were cut from each composition (with an average thickness of 20 μm) into rectangles having the length of 2 cm and width of 2 mm and tested. The test was done under controlled conditions of 23°C and 50% RH and average values for Young's modulus, tensile strength, and strain-at-break are reported using data collection from the 5 specimens.

Conductivity Measurements: The electrical conductivity of the nanopapers using a 2-point probe technique was measured. The films were cut into defined rectangular strips with known dimensions (2 mm wide and 2 cm long) and the two edges of the samples were silver-painted to provide good contact between a metal probe and the film, and the electrical resistance of each film was measured using SourceMeter 2401 (KEITHLEY, Beaverton, USA). The cyclic folding test was done by folding a structure with 3 parallel lines. The nanopaper was folded from 3 points of $+180^\circ$ and -180° and then again unfolded to ensure folding from each direction did not damage the CNT network in the patterns, and the conductivity was measured after each 100 folding–unfolding cycles.

SEM Imaging: Scanning electron microscopy (SEM) images were captured using the high-vacuum field-emission SEM (Hitachi S-4800, Hitachi Corp., Japan). The samples were fixed on a metal stub and coated with 4 nm layer of gold–palladium coating using Cressington

208HR (Watford, UK) sputter and imaging was performed with the working distance of 4–5 mm, secondary electron detector, 1 kV in acceleration voltage, and the probe current of 5 μ A.

AFM Imaging: Images were captured using a Multimode 8 atomic force microscope (AFM) from Bruker Corp., USA. The scanning was performed using RTESP cantilevers having a nominal tip radius of 8 nm and a spring constant of 5 N m^{-1} (Bruker CORP., USA). The edge of the pattern of the nanopaper was spotted using an in situ optical microscope and then the tip of the cantilever was put on the edge and surface roughness was measured as the root mean square (RMS) value of the whole scanned area $5 \times 5 \mu m^2$.

Cyclic Voltammetry: Copper wires were contacted to the symmetrical electrodes as the current collectors, using silver paint as conductive glue. The contact points were protected with epoxy resin and the interdigitated part was left uncovered, aqueous electrolyte of $100 \times 10^{-3} M K_3[Fe(CN)_6]$ was dropped in 1 \times PBS onto the surface of the area with interdigitated electrodes, and the device was covered with a petri dish in order to minimize the evaporation of water. CV of the device was performed at different scan rates with a VSP potentiostat/galvanostat (Bio-Logic Science Instruments, France) using a two-electrode setup.

Dispersion of CNF–AgNWs: AgNWs were purchased from Sigma-Aldrich as suspensions in isopropyl alcohol. The AgNWs were decanted for 3 days and the alcohol was removed from the top and then the earlier-prepared aqueous CNF dispersion was added in a given composition (60 wt% AgNWs) followed by sonication at 750 W and 30% amplitude in ice bath with a probe tip diameter of 4 mm for 2 min using Vibra-Cell CV33 (Sonics & Materials Inc., Newton, USA).

Supporting Information

Supporting Information is available from the Wiley Online Library or from the author.

Acknowledgements

The authors would like to acknowledge funding from Knut and Alice Wallenberg foundation through Wallenberg Wood Science Center.

Conflict of Interest

The authors declare no conflict of interest.

Keywords

carbon nanotubes, nanocelluloses, nanopapers, nanowires, printed electronics

Received: December 11, 2018
Published online:

- [1] S. R. Forrest, *Nature* **2004**, 428, 911.
- [2] A. Kamyshny, S. Magdassi, *Small* **2014**, 10, 3515.
- [3] S. Park, M. Vosguerichian, Z. Bao, *Nanoscale* **2013**, 5, 1727.
- [4] B. Y. Ahn, E. B. Duoss, M. J. Motala, X. Guo, S.-I. Park, Y. Xiong, J. Yoon, R. G. Nuzzo, J. A. Rogers, J. A. Lewis, *Science* **2009**, 323, 1590.
- [5] M. Berggren, D. Nilsson, N. D. Robinson, *Nat. Mater.* **2007**, 6, 3.
- [6] H. W. Choi, T. Zhou, M. Singh, G. E. Jabbour, *Nanoscale* **2015**, 7, 3338.
- [7] E. B. Secor, S. Lim, H. Zhang, C. D. Frisbie, L. F. Francis, M. C. Hersam, *Adv. Mater.* **2014**, 26, 4533.
- [8] W. J. Hyun, E. B. Secor, G. A. Rojas, M. C. Hersam, L. F. Francis, C. D. Frisbie, *Adv. Mater.* **2015**, 27, 7058.
- [9] K. Tybrandt, F. Stauffer, J. Vörös, *Sci. Rep.* **2016**, 6, 25641.
- [10] Y. Lin, D. Gritsenko, Q. Liu, X. Lu, J. Xu, *ACS Appl. Mater. Interfaces* **2016**, 8, 20501.
- [11] D. Jang, D. Kim, B. Lee, S. Kim, M. Kang, D. Min, J. Moon, *Adv. Funct. Mater.* **2008**, 18, 2862.
- [12] D. Tobjörk, R. Österbacka, *Adv. Mater.* **2011**, 23, 1935.
- [13] L. Hu, J. W. Choi, Y. Yang, S. Jeong, F. La Mantia, L.-F. Cui, Y. Cui, *Proc. Natl. Acad. Sci. USA* **2009**, 106, 21490.
- [14] H. Zhu, S. Parvinian, C. Preston, O. Vaaland, Z. Ruan, L. Hu, *Nanoscale* **2013**, 5, 3787.
- [15] X. Xu, J. Zhou, L. Jiang, G. Lubineau, T. Ng, B. S. Ooi, H.-Y. Liao, C. Shen, L. Chen, J. Zhu, *Nanoscale* **2016**, 8, 12294.
- [16] M. Henriksson, L. A. Berglund, P. Isaksson, T. Lindström, T. Nishino, *Biomacromolecules* **2008**, 9, 1579.
- [17] H. Zhu, Z. Fang, C. Preston, Y. Li, L. Hu, *Energy Environ. Sci.* **2014**, 7, 269.
- [18] M. Nogi, S. Iwamoto, A. N. Nakagaito, H. Yano, *Adv. Mater.* **2009**, 21, 1595.
- [19] F. Hoeng, A. Denneulin, J. Bras, *Nanoscale* **2016**, 8, 13131.
- [20] J. Huang, H. Zhu, Y. Chen, C. Preston, K. Rohrbach, J. Cumings, L. Hu, *ACS Nano* **2013**, 7, 2106.
- [21] H. Koga, T. Saito, T. Kitaoka, M. Nogi, K. Suganuma, A. Isogai, *Biomacromolecules* **2013**, 14, 1160.
- [22] Y. Fujisaki, H. Koga, Y. Nakajima, M. Nakata, H. Tsuji, T. Yamamoto, T. Kurita, M. Nogi, N. Shimidzu, *Adv. Funct. Mater.* **2014**, 24, 1657.
- [23] T. Inui, H. Koga, M. Nogi, N. Komoda, K. Suganuma, *Adv. Mater.* **2015**, 27, 1112.
- [24] Y. Song, Y. Jiang, L. Shi, S. Cao, X. Feng, M. Miao, J. Fang, *Nanoscale* **2015**, 7, 13694.
- [25] M.-C. Hsieh, C. Kim, M. Nogi, K. Suganuma, *Nanoscale* **2013**, 5, 9289.
- [26] R. Shenhar, T. B. Norsten, V. M. Rotello, *Adv. Mater.* **2005**, 17, 657.
- [27] K. Dick, T. Dhanasekaran, Z. Zhang, D. Meisel, *J. Am. Chem. Soc.* **2002**, 124, 2312.
- [28] D. Tobjörk, H. Aarnio, P. Pulkkinen, R. Bollström, A. Määttänen, P. Ihalainen, T. Mäkelä, J. Peltonen, M. Toivakka, H. Tenhu, R. Österbacka, *Thin Solid Films* **2012**, 520, 2949.
- [29] T. Benselfelt, J. Engström, L. Wågberg, *Green Chem.* **2018**, 20, 2558.
- [30] A. Russo, B. Y. Ahn, J. J. Adams, E. B. Duoss, J. T. Bernhard, J. A. Lewis, *Adv. Mater.* **2011**, 23, 3426.
- [31] F. Hoeng, A. Denneulin, G. Krosnicki, J. Bras, *J. Mater. Chem. C* **2016**, 4, 10945.
- [32] F. Hoeng, A. Denneulin, N. Reverdy-Bruas, G. Krosnicki, J. Bras, *Appl. Surf. Sci.* **2017**, 394, 160.
- [33] H. Zhu, Y. Li, Z. Fang, J. Xu, F. Cao, J. Wan, C. Preston, B. Yang, L. Hu, *ACS Nano* **2014**, 8, 3606.
- [34] M. M. Hamed, A. Hajian, A. B. Fall, K. Håkansson, M. Salajkova, F. Lundell, L. Wågberg, L. A. Berglund, *ACS Nano* **2014**, 8, 2467.
- [35] A. Hajian, S. B. Lindström, T. Pettersson, M. M. Hamed, L. Wågberg, *Nano Lett.* **2017**, 17, 1439.
- [36] A. Malti, J. Edberg, H. Granberg, Z. U. Khan, J. W. Andreasen, X. Liu, D. Zhao, H. Zhang, Y. Yao, J. W. Brill, *Adv. Sci.* **2016**, 3, 1500305.
- [37] G. Nyström, A. Mihranyan, A. Razaq, T. Lindström, L. Nyholm, M. Strømme, *J. Phys. Chem. B* **2010**, 114, 4178.
- [38] H. Sehaqui, A. Liu, Q. Zhou, L. A. Berglund, *Biomacromolecules* **2010**, 11, 2195.
- [39] Y. Yi, L. Berhan, A. Sastry, *J. Appl. Phys.* **2004**, 96, 1318.
- [40] T. Saito, S. Kimura, Y. Nishiyama, A. Isogai, *Biomacromolecules* **2007**, 8, 2485.
- [41] M. F. De Volder, S. H. Tawfick, R. H. Baughman, A. J. Hart, *Science* **2013**, 339, 535.

- [42] L. Hu, H. S. Kim, J.-Y. Lee, P. Peumans, Y. Cui, *ACS Nano* **2010**, *4*, 2955.
- [43] L. Hu, H. Wu, Y. Cui, *MRS Bull.* **2011**, *36*, 760.
- [44] Y. Lin, C. Cooper, M. Wang, J. J. Adams, J. Genzer, M. D. Dickey, *Small* **2015**, *11*, 6397.
- [45] M. M. Hamed, A. Ainla, F. Güder, D. C. Christodouleas, M. T. Fernández-Abedul, G. M. Whitesides, *Adv. Mater.* **2016**, *28*, 5054.
- [46] K. Tybrandt, J. Vörös, *Small* **2016**, *12*, 180.
- [47] H. Koga, M. Nogi, N. Komoda, T. T. Nge, T. Sugahara, K. Suganuma, *NPG Asia Mater.* **2014**, *6*, e93.
- [48] M. Nogi, M. Karakawa, N. Komoda, H. Yagyu, T. T. Nge, *Sci. Rep.* **2015**, *5*, 17254.
- [49] W. Dang, V. Vinciguerra, L. Lorenzelli, R. Dahiya, *Flexible Printed Electron.* **2017**, *2*, 013003.
- [50] F. J. Tölle, M. Fabritius, R. Mülhaupt, *Adv. Funct. Mater.* **2012**, *22*, 1136.
- [51] C. Yang, H. Gu, W. Lin, M. M. Yuen, C. P. Wong, M. Xiong, B. Gao, *Adv. Mater.* **2011**, *23*, 3052.
- [52] A. C. Siegel, S. T. Phillips, M. D. Dickey, N. Lu, Z. Suo, G. M. Whitesides, *Adv. Funct. Mater.* **2010**, *20*, 28.
- [53] L. Berhan, Y. Yi, A. Sastry, E. Munoz, M. Selvidge, R. Baughman, *J. Appl. Phys.* **2004**, *95*, 4335.
- [54] R. Mao, S. Goutianos, W. Tu, N. Meng, G. Yang, L. A. Berglund, T. Peijs, *J. Mater. Sci.* **2017**, *52*, 9508.
- [55] R. Picu, *Soft Matter* **2011**, *7*, 6768.
- [56] H. Ragones, D. Schreiber, A. Inberg, O. Berkh, G. Kósa, A. Freeman, Y. Shacham-Diamand, *Sens. Actuators, B* **2015**, *216*, 434.
- [57] G. Schwartz, B. C.-K. Tee, J. Mei, A. L. Appleton, D. H. Kim, H. Wang, Z. Bao, *Nat. Commun.* **2013**, *4*, 1859.
- [58] S. Zhang, R. Geryak, J. Geldmeier, S. Kim, V. V. Tsukruk, *Chem. Rev.* **2017**, *117*, 12942.
- [59] K. Yamada, T. G. Henares, K. Suzuki, D. Citterio, *Angew. Chem., Int. Ed.* **2015**, *54*, 5294.
- [60] C. Dixon, J. Lamanna, A. R. Wheeler, *Adv. Funct. Mater.* **2017**, *27*, 1604824.
- [61] M. M. Hamed, B. Ünal, E. Kerr, A. C. Glavan, M. T. Fernandez-Abedul, G. M. Whitesides, *Lab Chip* **2016**, *16*, 3885.
- [62] E. Morales-Narváez, H. Golmohammadi, T. Naghdi, H. Yousefi, U. Kostiv, D. Horák, N. Pourreza, A. Merkoçi, *ACS Nano* **2015**, *9*, 7296.
- [63] C. Xie, F. Yan, *Small* **2017**, *13*, 1701822.
- [64] A. M. Gaikwad, D. A. Steingart, T. Nga Ng, D. E. Schwartz, G. L. Whiting, *Appl. Phys. Lett.* **2013**, *102*, 233302.